Li *et al. J Mater. Sci: Mater Eng.* (2024) 19:44
https://doi.org/10.1186/s40712-024-00191-7

Journal of Materials Science: Materials in Engineering

ORIGINAL PAPER

Open Access

Study of SERS activity of different gold nanostructures prepared by electron beam lithography

Hao Li[1], Gen Liu[1,4], Yi Zhang[1], Luzhen Hao[1], Pinggen Zou[1], Yuchen Xu[1], Mei Ji[1], Xue Yu[1], Jiangli Li[1], Yanqing Ma[1,2,3*] and Lei Ma[1,2*]

Abstract

Plasmonic metal nanostructure prepared by photolithography technology can be used as a uniform and stable substrate with high SERS activity. However, there is only limited research on the precisely regulated metal nanostructures and the systematic studies on the relation between the structure and SERS response. Herein, different gold nanostructure arrays (including circles, equilateral triangles, squares, regular pentagons, regular hexagons, pentagrams, and hexagram) have been prepared using electron beam lithography (EBL). Rhodamine B were employed as the probe molecule. The effect of the shapes, sizes (s), spacing (d), and rotation angle (α) of different shapes gold on SERS activities were systematically investigated under the excitation of 532 nm laser. Further finite element method based electromagnetic field simulations unveiled the correlation between the local electromagnetic field strengths and the SERS activities, which also verified the proportional relation between the fourth power of the electromagnetic field intensity (L_E) and enhancement factor (EF).

Keywords SERS, Electron beam lithography, Gold nanostructure arrays, Electromagnetic field intensity, Enhancement factor

Introduction

Since the discovery (Fleischmann and A.J. 1974) of Surface-Enhanced Raman Scattering (SERS) phenomenon on rough silver electrodes by Fleischmann et al. in the 1970s, SERS has been proved to be an extremely sensitive technique for single-molecule detection, such as the thermoelectric materials (Zhang et al. 2024a; Tan et al. 2023; Shao et al. 2023), chemical sensing, biology, and medicine (Liu et al. 2024; Kneipp et al. 1997; Nie 1997; Yin et al. 2010; Dutta Roy et al. 2015; Yaseen et al. 2018; Tran et al. 2021; Beeram et al. 2023; Eremina et al. 2024; Wei et al. 2024; Zhang et al. 2024b).

Currently, to improve SERS performance, many researchers are committed to design and develop highly active SERS response substrates. Song et al. (Song et al. 2013) prepared highly branched gold nanoflowers through chemical synthesis methods and obtained highly active SERS active substrates. Silvia et al. (Barbosa et al. 2010) synthesized gold nanoparticles of different sizes and studied the relationship between their size and SERS performance. Joseph et al. (Joseph et al. 2007) still obtained the changes in SERS intensity at different

*Correspondence:
Yanqing Ma
mayanqing@tju.edu.cn
Lei Ma
lei.ma@tju.edu.cn
[1] Tianjin International Center for Nanoparticles and Nanosystems, Tianjin University, Nankai District, 92 Weijin Road, Tianjin 300072, People's Republic of China
[2] Tianjin Key Laboratory of Low-Dimensional Electronic Materials and Advanced Instrumentation, Tianjin 300072, People's Republic of China
[3] School of Precision Instrument and Opto-Electronics Engineering, Tianjin University, Tianjin 300072, People's Republic of China
[4] College of Physics and Electronic Engineering, Taishan University, Taian, Shandong 271000, China

sharp angles by chemically synthesizing silver nanocubes with different sharp angles. However, chemical synthesis methods are prone to introducing other impurities and cannot accurately control the synthesis of various nanostructures. Therefore, it is necessary to find a new method for preparing nanostructures.

Generally, there are two main methods to prepare SERS substrates: the wet chemical synthesis (Tiwari et al. 2007) and the top-down approaches (Yannick Sonnefraud et al. 2010; Ahmad et al. 2014). The wet chemical synthesis includes chemical synthesis of metal nanoparticles, nanorods, nanosheets, and their self-assemblies. Although wet chemical synthesis has the advantages of low cost and high local SERS response, it is difficult to achieve large-scale ordered structures, and mostly they suffer from the contamination (Chen et al. 2011) introduced in chemical process. In contrast, modern nanofabrication technique based top-down methods can easily realize structure precisely controlled SERS active substrates and barely impurities introduction, therefore uniform, stable, and reproducible SERS responses (Muhlschlegel et al. 2005; Kessentini et al. 2014). EBL technology has natural advantages in the preparation of metal nanostructures. Yu et al. (Qiuming et al. 2008) used EBL technology to precisely control the diameter and spacing of gold nanopores and studied their relationship with SERS performance. Jonas et al. (Beermann et al. 2009) prepared gold nanoparticle arrays of different sizes using EBL technology, revealing a good correspondence between reflection spectrum dependence and local SERS enhancement. Jenny et al. (Oran et al. 2008) investigated the SERS performance of gold nanoparticle arrays with different shapes and sizes using EBL technology. Therefore, EBL technology is a good choice for preparing SERS active substrates. However, most of reported works focus on obtaining high SERS activity substrates, lacking systematic experimental investigation on structure-performance of such system. It should be thoroughly explored through precisely fabricated metal nanostructures.

In this article, EBL technology was first used to accurately prepare different gold nanostructure arrays, achieving controllability of SERS active substrates. Subsequently, Rhodamine B (RhB) was used as a probe molecule, and the relationship between SERS activity response and different gold nanostructure arrays was systematically studied under 532 nm excitation laser. The results were further elucidated by using CST simulation calculations which verify the unveiled linear relationship between local electromagnetic field strength (L_E) and enhancement factor (EF).

Experimental methods

Preparation of SERS-active substrates

The prepared SiO_2/Si substrates (10 mm × 10 mm) were sequentially cleaned using acetone, ethanol, and Milli-Q water for 30 min in an ultrasonic bath, then dried with purified dry nitrogen gas. The electron beam lithography system (VEGA3, TESCAN, Ltd.) was used to create patterns of different nanostructure arrays on the cleaned SiO_2/Si substrate surfaces. 5 nm Cr and 10 nm Au layer were deposited consecutively using an electron beam evaporation system (EBD, DZS500, Co., Ltd. CAS) (supporting information for details). The samples were then subjected to a lift-off process to form nanostructure arrays. The detailed preparation process is shown in Fig. 1 (taking the pentagram structure as an example). Subsequently, the prepared samples were immersed in a 10^{-6} mol L^{-1} RhB solution for 3 h, rinsed with deionized water. The resulting samples were dried in air and used for further characterization and SERS measurements.

Morphology characterization

The morphology of the metal nanostructures was characterized using a scanning electron microscope (SEM, SU3500, Hitachi, Japan) at an accelerating voltage of 15 kV and a working distance of 6 mm. The sample profile of Z-height was measured using atomic force

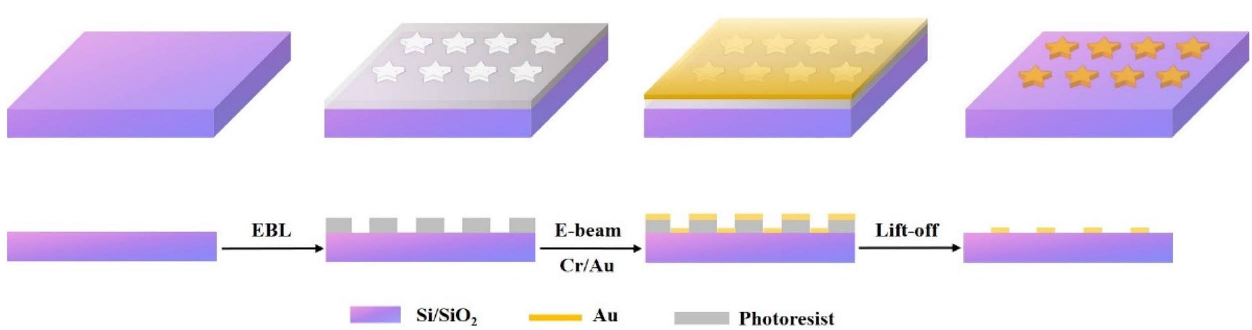

Fig. 1 Schematic diagram of EBL preparation process for SERS active substrates with different structures

microscopy (AFM, Korea Park X-10 Systems) in the non-contact mode (NCM).

Raman measurements

SERS measurements were **c**onducted using a confocal microscope spectrometer (RTS-2, Titan Electro-Optics (Hong Kong) Ltd) with a 50 × long focal length objective lens and excitation laser of 532 nm. All Raman spectra were acquired with an integration time of 5 s, and five spots are taken in each 50 μm × 50 μm patterned area. In all experiments, the laser power was 0.3 mW.

Calculation of the enhancement factor

The three SERS EFs are single-molecule EF, substrate EF, and analytical EF (Natan 2006; Le et al. 2007; Dey 2023). The analytical can be defined as:

$$EF = \left(\frac{I_{SERS}}{I_{REF}}\right) \times \left(\frac{C_{REF}}{C_{SERS}}\right) \quad (1)$$

where I_{SERS} and I_{REF} are the measured Raman signal intensity of featured peaks from the probe molecule with and without SERS active substrate, respectively. C_{SERS} and C_{REF} are the concentration of the probe molecule before testing the SERS substrate (10^{-6} mol L^{-1}) and the SiO_2/Si substrate (0.1 mol L^{-1}), respectively.

Simulation calculations

The significant enhancement of Raman scattering is generally attributed to electromagnetic and charge transfer mechanism (Heller 1982; Shamsali et al. 2023; Lombardi et al. 1986; Dong et al. 2023), which often coexist. For most noble metal systems, the electromagnetic field enhancement is dominant which is mainly resulted by the surface plasmon resonance (SPR) (Gersten 1980) of the metal nanostructures. The optimal local electromagnetic field strengths are realized by matching laser frequency to the SPR frequency of the nanostructure (Li et al. 2008). Therefore, unveiling structure -performance relation is essential for developing and fabricating appropriate metal nanostructures to maximize the SPR electromagnetic field effect (Maier 2006).

The SERS response roots to the enhancement of the electromagnetic fields resulted by gold nanostructure plasmon resonances. As an effective simulation tool, the CST software was applied to investigate the distribution of the local field enhancement (L_E) and its relationship with EF on the EM irritated periodic nanostructures (Chakraborty et al. 2021; Goel et al. 2021; Ko and Chen 2022). According to the classical theory, the EF is proportion to L_E^4, $L_E = E_{loc}/E_o$, where E_o and E_{loc} are the local electric field strength on the nanostructure with and without resonance, respectively[50]. The CST simulation process is listed in the supporting information.

Results and discussion

Gold nanostructures with different shapes

As shown as in Fig. 2 (I), gold nanostructure arrays with different shapes have been successfully prepared on SiO_2/Si substrate using EBL, including circles (Cir), triangles(Tri), squares (Squ), pentagons (Pen), hexagons (Hex), pentagonal star (Ps), and hexagonal star (Hs). They all have square lattice with constant of d = 150 ± 5 nm and s = 400 ± 5 nm. The corresponding AFM characterizations of the samples are shown in Figure S1 (I) which indicate that the height of each structure is h = 15 ± 5 nm.

As illustrated in Fig. 2 (II) and (III), the arrays with pentagram and circular elements demonstrate the highest and lowest SERS response of RhB molecule among all test structures (s = 400 nm, d = 150 nm) with the value of EF 3.57×10^6 and 6.11×10^4, respectively. The calculation of EF was conducted using the intensity of the peak at 1649 cm^{-1} as a reference. The results also show that the sharper of the conners or tips, the more the tips and the sides, the larger the EF will be. It is consistent with the previous reported results(36). Due to the sharper angle, the gaps between structural elements on the outer surface are larger. It can be resulting in denser charge accumulation and stronger electric field strength. Therefore, the more tips there are, the stronger the electric field strength. In addition, when the laser is irradiated, the charges are mainly concentrated at the tip, there are also charges at the edges. So, the more sides, the stronger the electric field strength. The size of EF depends on the strength of the electric field. And the stronger the electric field, the larger the EF.

To investigate the relationship between the localized electromagnetic field intensity and EF, the CST software was used to simulate the strength of the resonant electromagnetic field generated by different gold nanostructure arrays in Fig. 2 (IV). The results indicate that the fitting of electromagnetic field intensity matches the EF value. The relationship between L_E and EF has been further studied as shown in Figure S2 (a) which indicates EF and L_E^4 are nicely linearly correlated.

To further elucidate the relationship between EF and angle (β) and quantity (n) (angles and sides), a quantitative relationship between EF and β and n was established through multiple linear regression (The detailed fitting process can be found in the supporting information Table S1). To study the contribution of convex and concave angles and sides to EF, an empirical model is developed and presented as Eq. (2).

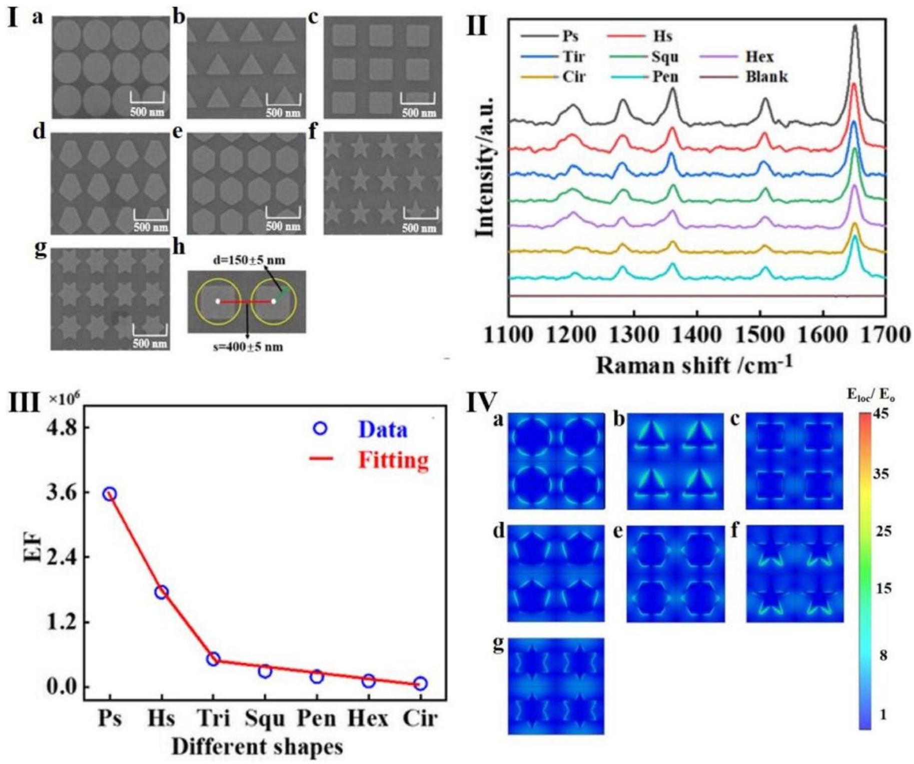

Fig. 2 Gold nanostructure arrays with different shapes: (I) SEM images (**a**) Circular array, (**b**) Triangle array, (**c**) Square array, (**d**) Pentagon array, (**e**) Hexagon array, (**f**) Pentagonal star array, (**g**) Hexagonal star array, (**h**) SEM size diagram; (II) Measured Raman spectra of RhB molecule on different gold structure arrays. Five observable Raman shifts at 1196 cm^{-1}, 1275 cm^{-1}, 1350 cm^{-1}, 1506 cm^{-1} and 1646 cm^{-1}. For 1646 cm^{-1}, 1350 cm^{-1} and 1275 cm^{-1} reflect the stretching vibrations of carbon–carbon double bonds in the benzene ring. The one at 1196 cm^{-1} and 1506 cm^{-1} are the results of the deformation vibration of the benzene ring and vibration of the carbon-hydrogen bond, respectively (Jia and Z. XL, X. Ming 2005; Yan et al. 2015; Seçkin et al. 2023); (III) The enhancement factors with the reference the intensity of the peak at 1649 cm^{-1} and fitting results; (IV) Simulation results of local electromagnetic field intensity (E_{loc}/E_O) response of different gold nanostructures

$$\mathrm{EF} = a_1 \times \frac{n_1}{(\beta_1)^2} + a_2 \times n_2 \times \beta_2 + a_3 \times n_3 + a \tag{2}$$

The first term and the second term represent the contribution of the convex angle and the concave angle to EF, respectively, and the term a is for taking care all other influences which cannot be attributed to the first two terms. The fitting result is shown in Fig. 2 (III), where the parameters are $a_1 = 8.62 \times 10^8$, $a_2 = 4.00 \times 10^2$, $a_3 = 0$ and $a = -2.21 \times 10^5$.

Different pentagram shaped gold nanostructure arrays

As discussed in above sections, the correlation among the adjacent units is included in the term a. In order to further clarify this part, pentagram-shape gold arrays with different spacings (s), sizes (d), and rotation angles (α) (α is the counterclockwise rotation angle from an initial angle of 0°) were prepared. The corresponding AFM characterizations of the samples are shown in Figure S1 (II).

Figure 3 shows the results of pentagram shaped with different s. The SEM of Fig. 3 (I) indicates the successful preparation of pentagram shaped arrays with different s. The SERS test results are shown in Fig. 3 (II). The smaller the spacing, the stronger the SERS response, as shown in Fig. 3 (III) that the EF increases as the spacing between the pentagrams in the array decreased with negative linear correlation in formula (3) where $b_1 = -4.00 \times 10^3$, $b = 3.868 \times 10^6$. (The detailed fitting process can be found in the supporting information Table S2). This is consistent with the results of Christy et al. (Duyne 2003).

$$\mathrm{EF} = b_1 \times s + b \tag{3}$$

Figure 3 (IV) shows that the fitting results of the electromagnetic field intensity are consistent with the experimental results which is consistent with the results of Amy et al. (Amy et al. 1999) and Chao et al. (Chao et al. 2015). The data in this work compared with previous work is listed in the Table S3.

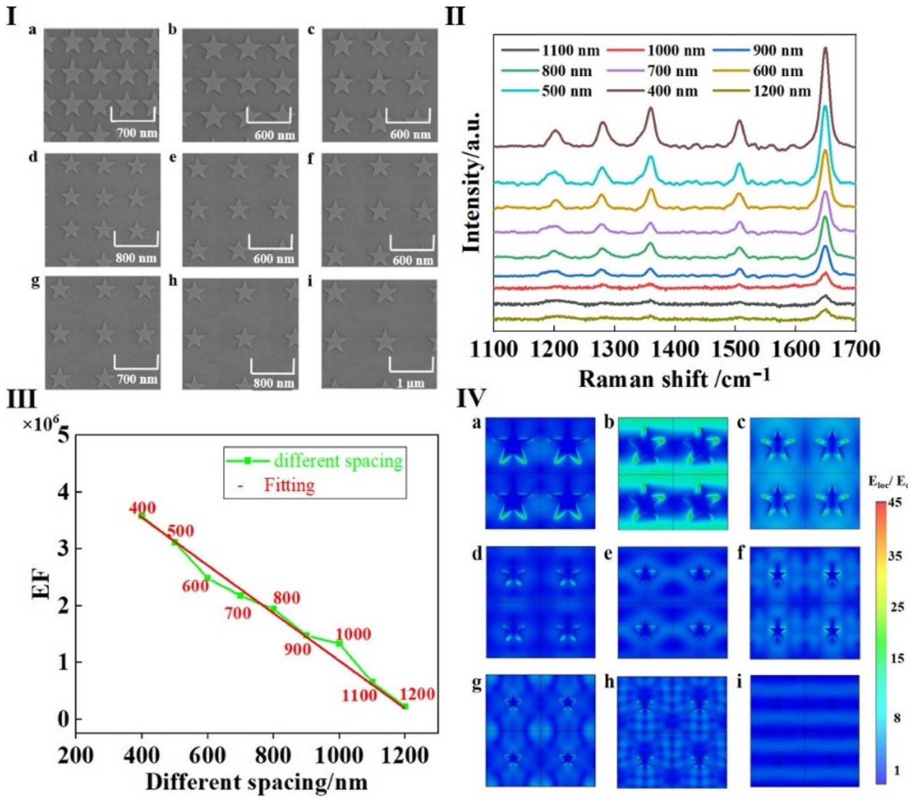

Fig. 3 Pentagram shaped arrays with different spacing(s): (I) SEM images, (**a**) 400 nm, (**b**) 500 nm, (**c**) 600 nm, (**d**) 700 nm, (**e**) 800 nm, (**f**) 900 nm, (**g**) 1000 nm,(**h**) 1100 nm, and (**i**) 1200 nm; (II) Measured Raman spectra of RhB molecule with different s; (III) The enhancement factors with the reference the intensity of the peak at 1649 cm^{-1} and fitting results (IV) Simulation results of local electromagnetic field intensity (E_{loc}/E_o) response with differents

Further research was conducted on the influence of pentagram shaped arrays with different sizes (d) and rotation angles (α) on SERS response. The test results are shown in Figures S3 and S4 in the supporting information. The results indicate that both d and α have an impact on SERS response. The influence of size may be the reason for laser wavelength matching, while the influence of angle factor needs further exploration.

Normalizing formulas (2) and (3) can be approximated as

$$EF = (b_1 \times s + b) \times \left\{ a_1 \left[\frac{n_1}{(\beta_1)^2} \right] + a_2 \times n_2 \times \beta_2 + a \right\} / 3.57 \quad (4)$$

It is known that the main factors affecting EF are spacing, angle and number of external convex angles.

To verify the validity of Formula (4), we further prepared a "gear like" structure and conducted SERS testing. Randomly select 4 points in the array for SERS response testing, and the test results are basically consistent, indicating the uniformity and stability of the active substrate as shown in Fig. 4 (b). The equation predicted EFs well match the experimentally measured ones in Fig. 4 (c), with a standard deviation of less than 2.8% in Fig. 4 (d) which verifies the accountability of the empirical formula.

Conclusion

In conclusion, different gold nanostructure arrays have been successfully prepared using EBL technology, and accurate regulation of the active substrate structure of SERS has been achieved. This method avoids the influence of surface impurities that may be present when preparing SERS substrates using chemical synthesis, making it significant for systematically studying the impact of different gold nanostructures on SERS response. The influence of different shaped gold nanostructures on the SERS response was investigated using RhB as a probe molecule. The results indicate that different shapes of gold nanostructures have a significant impact on EF. Furthermore, the study of the impact of different spacings (s) of pentagram-shaped gold nanostructures on the SERS

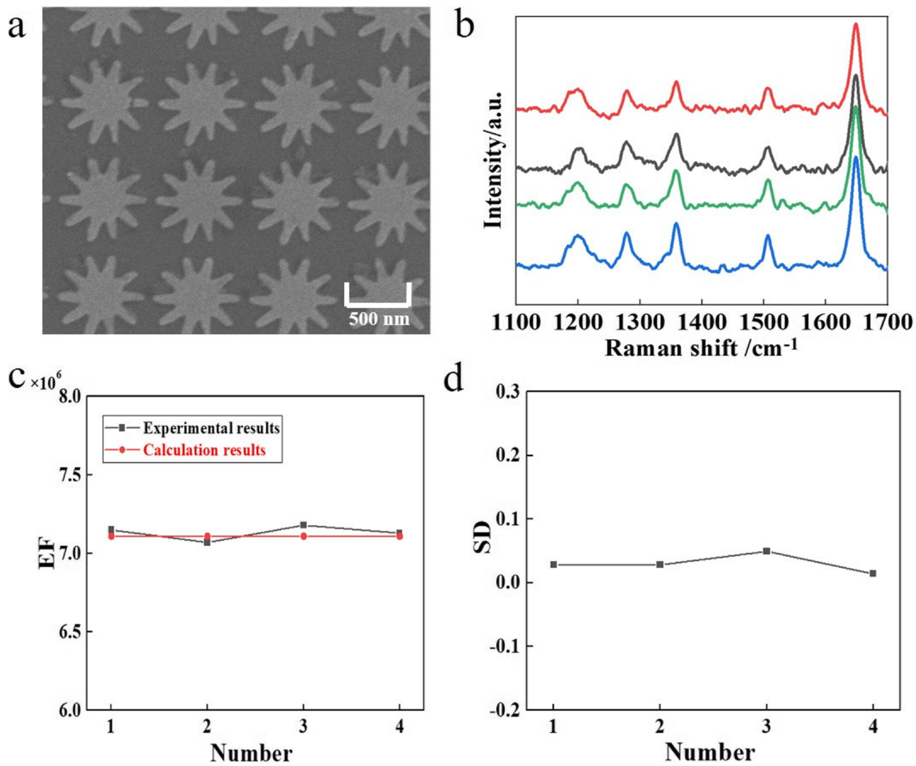

Fig. 4 Verification of calculation results: (**a**) SEM image and (**b**) SERS result (different colored lines represent different testing points) of the "gear like" structure. (**c**) Comparison of EF ("number" is the number of measured points, the black line represents experimental data, and the red line represents predicted data) (**d**) SD of experimental and computational data in (c)

response showed that the SERS response increased as the s decreased. The main factors affecting EF are spacing, angle and number of external convex angles.

This work systematically studied the relationship between SERS substrate activity and structure, providing reference for the further design and development of high active SERS substrates.

Supplementary Information

The online version contains supplementary material available at https://doi.org/10.1186/s40712-024-00191-7.

Supplementary Material 1.

Acknowledgements

This work was financially supported by The National Key R&D Program of China (No. 2022YFC3006303).

Authors' contributions

Hao Li: Data curation, formal analysis, investigation, writing – original draft. Gen Liu, Yi Zhang, Luzhen Hao: Formal analysis. Pinggen Zou: Software, Yuchen Xu: Methodology. Mei Ji and Jiangli Li: Formal analysis. Yanqing Ma: Funding acquisition, validation, writing – review & editing. Lei Ma: Funding acquisition, conceived and supervised project, writing – review & editing.

Data availability

All data and code generated or used during the study appear in the submitted article.

Declarations

Ethics approval and consent to participate

There are no experiments involving human tissue in this article.

Competing interests

The authors declare that they have no known competing financial interests or personal relationships that could have appeared to influence the work reported in this paper.

Received: 12 July 2024 Accepted: 17 November 2024
Published online: 04 December 2024

References

Ahmad N, Abbas GL, Bilu L, Luyao Z, He L, Douglas O, Wei W, Chongwu Z (2014) Patterning, characterization, and chemical sensing applications of graphene nanoribbon arrays down to 5 nm using helium ion beam lithography, ACS. NANO 8:1538–1546

Amy M, Michaels MN, Brus LE (1999) Surface enhanced raman spectroscopy of individual Rhodamine 6G molecules on large Ag nanocrystals. J Am Chem Soc 121:9932–9939

Barbosa S, Agrawal A, Rodriguez-Lorenzo L, Pastoriza-Santos I, Alvarez-Puebla RA, Kornowski A (2010) Tuning size and sensing properties in colloidal gold nanostars. Langmuir 26:14943–14950

Beeram R, Vepa KR, Soma VR (2023) Recent Trends in SERS-Based Plasmonic Sensors for Disease Diagnostics, Biomolecules Detection, and Machine Learning Techniques. Biosensors 13:1–37
Beermann J, Leosson K, Bozhevolnyi SI (2009) Surface enhanced Raman imaging periodic arrays and individual metal nanoparticles. Opt Express 17:12698–12705
Chakraborty S, Awasthi V, Goel R, Dubey SK (2021) Numerical design of SERS-active substrate for analyte detection using gold-hexagonal patterns. Vib Spectrosc 117:103312
Chao BK, Lin SC, Nien LW, Li JH, Hsueh CH (2015) Effects of corner radius on periodic nanoantenna for surface-enhanced Raman spectroscopy. J Opt 17:125002
Chen A, DePrince AE, Demortiere A, Joshi-Imre A, Shevchenko EV, Gray SK (2011) Self-assembled large Au nanoparticle arrays with regular hot spots for SERS. Small 7:2365–2371
Dey P (2023) Aiming for Maximized and Reproducible Enhancements in the Obstacle Race of SERS. ACS Measurement Science Au 3:434–443
Dong YM, Xie QH, Wu S, Li JB, Sun L, Ji W (2023) Revealing Adsorption Mechanism of p-Mercaptobenzoic Acid with TiO2 Surfaces Using Electric Field-Enhanced Semiconductor SERS. The Journal of Physical Chemistry C 127:9418–9424
Dutta Roy S, Ghosh M, Chowdhury J (2015) Adsorptive parameters and influence of hot geometries on the SERS spectra of methylene blue molecules adsorbed on gold nanocolloidal particles. J Raman Spectrosc. 46:451–461.
Duyne C (2003) Plasmon-sampled surface-enhanced Raman excitation spectroscopy. J Phys Chem B 107:7426–7433
Eremina OE, Yarenkov NR, Bikbaeva GI, Kapitanova OO, Samodelova MV, Shekhovtsova TN (2024) Silver nanoparticle-based SERS sensors for sensitive detection of amyloid-β aggregates in biological fluids. Talanta 266:124970
Fleischmann M, Mcquillan Raman AJ (1974) Spectra of pyridzne adsorbed at a silver electrode. Chem Phys Lett. 26:163–166.
Gersten JN (1980) Electromagnetic theory of enhanced Raman scattering by molecules adsorbed on rough surfaces. J Chem Phys 73:3023–3037
Goel R, Awasthi V, Rai P, Dubey SK (2021) Electrically tunable SERS active substrate exploiting electro-optic property of $LiNbO_3$ on Au-grating. Opt Mater 122:111735
Heller EJ (1982) Simple aspects of Raman scattering. J Phys Chem C 86:1822–1833
Jia TZ, XiaoLin X, Ming S (2005) Surface enhanced raman scattering effects of silver colloids with different shapes. J Phys Chem B 109:12544–12548.
Joseph M, McLellan YL, Andrew R (2007) Siekkinen, and Y. Xia, the SERS Activity of a Supported Ag Nanocube Strongly Depends on Its Orientation Relative to Laser Polarization, Nano Letters 7:1013–1017
Kessentini S, Barchiesi D, Andrea DC, Toma A, Guillot N, Fabrizio DE (2014) Gold dimer nanoantenna with slanted gap for tunable LSPR and improved SERS. The Journal of Physical Chemistry C 118:3209–3219
Kneipp WY, Kneipp H, Perelma LT, Itzkan I (1997) Single molecule detection using surface-enhanced Raman scattering (SERS). Phys Rev Lett 78:1667–1670
Ko TS, Chen YL (2022) Hybrid Enhancement of surface-enhanced raman scattering using few-layer MoS_2 decorated with au nanoparticles on Si nanosquare holes. Nanomaterials (Basel) 12:786
Le EC, Ru EB, Meyer M, Etchegoin PG (2007) Surface enhanced Raman scattering enhancement factors a comprehensive study. J Phys Chem C 111:13794–13803
Li K, Clime L, Cui B, Veres T (2008) Surface enhanced Raman scattering on long-range ordered noble-metal nanocrescent arrays. Nanotechnology 19:145305
Liu YH, Qiao SD, Fang C, He Y, Sun HY, Liu J, Ma YF (2024) A highly sensitive LITES sensor based on a multi-pass cell with dense spot pattern and a novel quartz tuning fork with low frequency. Opto-Electronic Advances 7:230230
Lombardi JR, Lu T, Xu J (1986) Charge transfer effects in surface-enhanced Raman scattering. J Chem Phys 84:4174–4180
Maier SA (2006) Plasmonic field enhancement and SERS in the effective mode volume picture. Opt Express 14:1957–1964
Muhlschlegel P, Martin OJF, Hecht B, Pohl DW (2005) Resonant optical antennas. Science 308:1607–1609
Natan MJ (2006) Concluding remarks surface enhanced Raman scattering. Faraday Discuss 132:321–328
Nie S (1997) Probing single molecules and single nanoparticles by surface-enhanced Raman scattering. Science 275:1102–1106
Oran JM, Hinde RJ, Abu NH, Retterer ST, Sepaniak MJ (2008) Nanofabricated periodic arrays of silver elliptical discs as SERS substrates. J Raman Spectrosc 39:1811–1820
Qiuming PG, Dong Q, Greg G, Paul M (2008) Wallace, Inverted size-dependence of surface-enhanced raman scattering on gold nanohole and nanodisk arrays. Nano Lett 8:1923–1928
Seçkin S, Singh P, Jaiswal A, and König AFT (2023) Super-Radiant SERS Enhancement by Plasmonic Particle Gratings. ACS Applied Materials & Interface. 15:43124–43134.
Shamsali F, Solovyeva EV, Nasiri N, Jamshidi Z (2023) How is the Observation of High-Order Overtones and Combinations Elucidated by the Charge-Transfer Mechanism in SERS. J Phys Chem A 127:10583–10590
Shao MR, Ji C, Tan JB, Du BQ, Zhao XF, Yu J, Man BY, Xu KC, Zhang C, Li Z (2023) Ferroelectrically modulate the Fermi level of graphene oxide to enhance SERS response. Opto-Electronic Advances 6:230094
Song HM, Deng L, Khashab NM (2013) Intracellular surface-enhanced Raman scattering (SERS) with thermally stable gold nanoflowers grown from Pt and Pd seeds. Nanoscale 5:4321–4329
Tan JB, Du BQ, Ji C, Shao MR, Zhao XF, Yu J, Xu SC, Man BY, Zhang C, Li Z (2023) Thermoelectric Field-Assisted Raman Scattering and Photocatalysis with GaN-Plasmonic Metal Composites. ACS Photonics 10:2216–2225
Tiwari VS, Oleg T, Darbha GK, Hardy W, Singh JP, Ray PC (2007) Non-resonance SERS effects of silver colloids with different shapes. Chem Phys Lett 446:77–82
Tran TH, Nguyen HT, Nguyen MH, Pham NH, Ngac AB, Mai HH (2021) Synthesis of ZnO/Au nanorods for self cleaning applications. J Nanosci Nanotechnol 21:2621–2625
Wei X, Song W, Fan Y, Sun Y, Li Z, Chen S (2024) A SERS aptasensor based on a flexible substrate for interference-free detection of carbendazim in apple. Food Chem 431:137120
Yan ZX, Zhang YL, Wang W, Fu XY, Jiang HB, Liu YQ (2015) Superhydrophobic SERS substrates based on silver-coated reduced graphene oxide gratings prepared by two-beam laser interference, ACS. Appl. Mater. Interfaces 7:27059–27065
Yannick Sonnefraud NV, Sobhani H, Guy AE, Vandenbosch VV, Moshchalkov DP Van, Nordlander P, and Stefan A (2010) Experimental realization of subradiant, superradiant, and fano resonances in ring disk plasmonic nanocavities. ACS Nano. 4:1664–1670.
Yaseen T, Pu H, Sun DW (2018) Functionalization techniques for improving SERS substrates and their applications in food safety evaluation, A review of recent research trends. Trends Food Sci Technol 72:162–174
Yin PG, Jiang L, You TT, Zhou W, Li L, Guo L (2010) Surface-enhanced Raman spectroscopy with self-assembled cobalt nanoparticle chains: Comparison of theory and experiment. Phys Chem Chem Phys 12:10781–10785
Zhang C, Tan JB, Du BQ, Ji C, Pei ZY, Shao MR, Jiang SZ, Zhao XF, Yu J, Man BY, Li Z, Xu KC (2024a) Reversible Thermoelectric Regulation of Electromagnetic and Chemical Enhancement for Rapid SERS Detection. ACS Appl Mater Interfaces 16:12085–12094
Zhang H, Tang Y, Wang W, Yu D, Yang L, Jiang X (2024b) A new semiconductor heterojunction SERS substrate for ultra-sensitive detection of antibiotic residues in egg. Food Chem 431:137163

Publisher's Note